Computer Vision and Image Understanding
Vol. 73, No. 3, March, pp. 441–454, 1999
Article ID cviu.1998.0738, available online at http://www.idealibrary.com on IDEAL®

Convexity Rule for Shape Decomposition Based on Discrete Contour Evolution

Longin Jan Latecki and Rolf Lakämper

Department of Applied Mathematics, University of Hamburg, Bundesstrasse 55, 20146 Hamburg, Germany
E-mail: latecki@math.uni-hamburg.de, lakaemper@math.uni-hamburg.de

Received January 21, 1998; accepted September 23, 1998

We concentrate here on decomposition of 2D objects into meaningful *parts of visual form*, or *visual parts*. It is a simple observation that convex parts of objects determine visual parts. However, the problem is that many significant visual parts are not convex, since a visual part may have concavities. We solve this problem by identifying convex parts at different stages of a proposed contour evolution method in which significant visual parts will become convex object parts at higher stages of the evolution. We obtain a novel rule for decomposition of 2D objects into visual parts, called the hierarchical convexity rule, which states that visual parts are enclosed by maximal convex (with respect to the object) boundary arcs at different stages of the contour evolution. This rule determines not only parts of boundary curves but directly the visual parts of objects. Moreover, the stages of the evolution hierarchy induce a hierarchical structure of the visual parts. The more advanced the stage of contour evolution, the more significant is the shape contribution of the obtained visual parts.

Key Words: **visual parts; discrete curve evolution; digital curves; digital straight line segments; total curvature; shape hierarchy; digital geometry.**

1. INTRODUCTION

We concentrate here on decomposition of 2D objects into meaningful parts. According to Siddiqi *et al.* [26],

> Part-based representations allow for recognition that is robust in the presence of occlusion, movement, deletion, or growth of portions of an object. In the task of forming high-level object-centered models from low-level image-based features, parts serve as an intermediate representation.

There is also a strong evidence for part-based representations in human vision, see [26] for an overview. Hoffman and Richards [12] provided strong evidence that contours are psychologically segmented at negative curvature minima. They stated the following rule (cited from Hoffman and Singh [13]):

> *Minima rule for silhouettes:* For any silhouette, all negative minima of curvature of its bounding curve are boundaries between parts.

Hoffman and Singh write [13]:

> ...the minima rule states in principle what these boundaries are, leaving open how in practice they may be computed from images despite noise and other resources.

One of the main motivations for our work was the question of how to robustly compute significant parts of boundaries from real digital images. In particular, since negative minima of curvature as well as other extremal points are obtained by local computation, their computation is not robust in real digital images.

Since objects we deal with in computer vision are mostly digital objects obtained by segmentation in digital images, our starting point was the discrete nature of digital objects. Therefore, we propose a multiscale shape decomposition rule which yields for many objects similar parts as in Hoffman and Richards [12]. However, we do not use extremal points of contour curves to compute the parts.

The presented approach to multiscale shape decomposition is based on shape hierarchy obtained by a discrete curve evolution. We present a novel approach to the evolution of digital planar curves that is based on digital linearization. In contrary to continuous curves, every digital curve is composed of digital line segments, which implies that every curve in a digital image can be regarded as a polygonal curve with a possible large number of vertices. We decompose a digital curve into maximal digital line segments.

The basic idea of the evolution is very simple: in every evolution step, we replace two consecutive line segments with a single line segment joining their endpoints. The key property of the evolution is the order of this substitution. If we do this in the "right" order, then we obtain an intuitive shape evolution of the curve. The substitution is done according to a relevance order of digital arcs that measures the significance of their contribution to the shape of the curve, beginning with arcs that contribute in the least significant way. This method allows us first to eliminate noise influence without changing the shape of objects. For example, compare the original curve (a) to curve (b) in Fig. 1.

If we continue to evolve the curve, we will linearize digital arcs that are relevant to the curve shape, which will result in a successive simplification of the curve shape. We use this shape simplification to derive a shape hierarchy for planar curves. For example, we obtain $(a) < (b) < \cdots < (f)$ as the shape hierarchy

1077-3142/99 $30.00

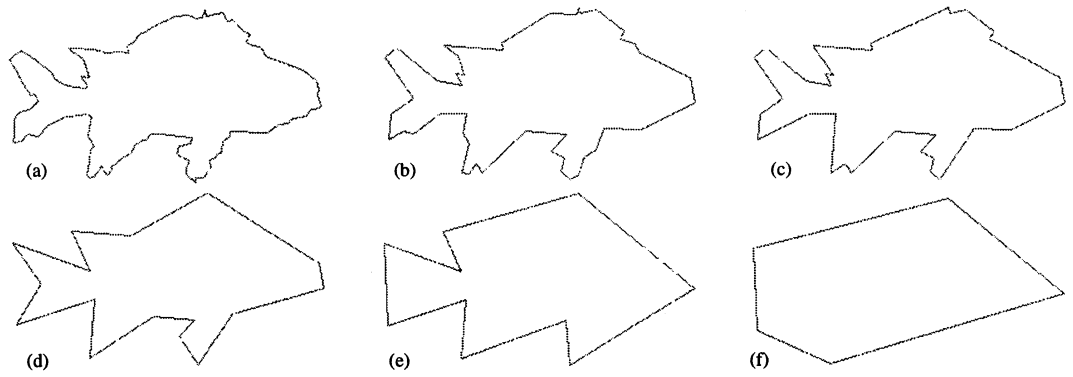

FIG. 1. A few stages of the proposed discrete curve evolution. Contour shown in (a) is a distorted version of the contour on the WWW page http://www.ee.surrey.ac.uk/Research/VSSP/imagedb/demo.html.

in Fig. 1. Since in every evolution step, the number of digital line segments in the curve decomposition decreases by one, the evolution converges to a convex polygon, which defines the highest level in the shape hierarchy, e.g., Fig. 1f. The presented evolution method is translation, rotation, reflection, and scaling invariant.

The obtained shape hierarchy is a base for object decomposition into relevant visual parts. The parts obtained on the highest levels of the hierarchy determine the most significant parts of the object. To decompose a digital curve into relevant parts on a given level of the shape hierarchy, we group the digital line segments of its boundary curve into maximal convex arcs.

The fact that visual parts are somehow related to convexity has been noticed in the literature; e.g., Basri *et al.* [1] state

> Parts generally are defined to be convex or nearly convex shapes separated from the rest of the object at concavity extrema, as in Hoffman and Richards [12], or at inflections, as in Koenderink and Doorn [15].

In Vaina and Zlateva [31] largest convex patches were used for part decomposition of 3D objects. Although the observation that visual parts are "nearly convex shapes" is very natural, the main problem is to determine the meaning of "nearly" in this context. We will present the details of our solution to this problem in Section 2. Now we state a few simple definitions.

We call maximal convex arcs *supported* arcs following Latecki and Rosenfeld [17]. We call finite unions of supported arcs *tame* arcs. Maximal supported arcs determine alternating and overlapping convex and concave parts of the object boundary. For example, Fig. 2 shows a decomposition of a polygonal curve into maximal supported arcs: the dashed arcs (inside the polygon) indicate the concave arcs with respect to the polygon while the dotted arcs (outside of the polygon) indicate the convex arcs with respect to the polygon. In the following, the term *maximal convex arc* denotes a supported arc that is convex with respect to the object.

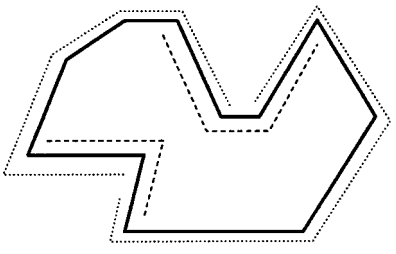

FIG. 2. Decomposition of a polygonal arc into maximal supported arcs.

Recall that we work with digital arcs, which can be treated as polygonal arcs without loss of information. Thus, we use polygonal definitions of the global curvature, which is equal to the total turn of a polygonal arc. The definition of the *global curvature* (or *total turn*) of a polygonal arc is illustrated in Fig. 3. This definition has been extended to digital arcs in Latecki and Rosenfeld [17].

2. SHAPE DECOMPOSITION

It is a simple and natural observation that maximal convex parts of objects determine visual parts. However, the problem is that many significant visual parts are not convex, since a visual part may have concavities. We solve this problem by identifying convex parts at different stages of the proposed contour evolution in which significant visual parts will become convex object parts at higher stages of the evolution: A significant visual part may have concavities, whose boundary parts are supported concave arcs. Since these concave arcs contribute in a less relevant way to the shape of the object than the boundary arc enclosing the significant visual part, the concavities will disappear in an earlier stage of the boundary evolution. Thus, there exists an evolution stage at which a significant visual part is a convex part. We base our approach to shape decomposition into visual parts on the following rule:

- *Hierarchical convexity rule.* The maximal convex arcs (w.r.t. the object) at various levels of the contour evolution determine parts of object boundary that enclose visual parts of the object.

The visual parts are determined on the original shape, i.e., it is not a maximal convex arc that is itself a visual part, but the

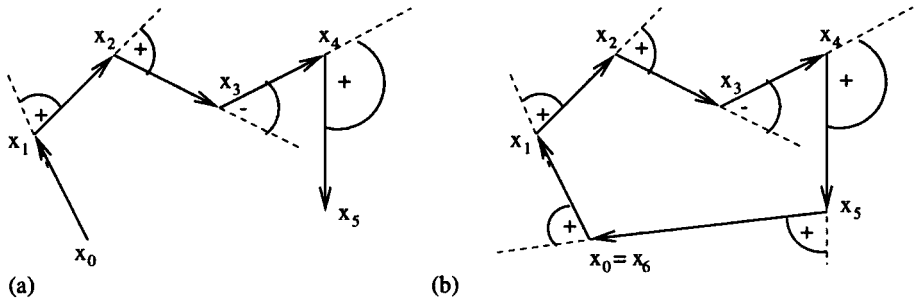

FIG. 3. (a) The *total turn* of a polygonal arc is the sum of turn angles at its vertices: $\tau(x_1) + \cdots + \tau(x_4)$. (b) For a closed polygonal arc, the total turn is $\tau(x_0) + \cdots + \tau(x_5)$.

piece of the original contour determined by the convex arc that encloses a visual part of the object. In other words, the endpoints of the maximal convex arc determine the piece of the original contour that encloses a visual part.

Figure 4 shows two examples of visual parts obtained by the proposed hierarchical convexity rule. On the highest level of the evolution hierarchy (a) in Fig. 4, the evolved silhouette of the "bear" is decomposed into three maximal convex arcs, and the evolved silhouette of the "fish" is decomposed into two maximal convex arcs. The visual parts enclosed by corresponding arcs on the original shape represent the most relevant object parts; those are the fish body and the tail for the fish and the upper body and legs together with hips for the bear. On one of the lower levels of the shape hierarchy (b) in Fig. 4, we obtain further visual parts, e.g., the head and the arms for the bear. The visual parts obtained by the hierarchical convexity rule on levels (a) and (b) are shown on the original contours in (c). Another example is given in Fig. 8, where the order of pictures follows the steps of the evolution.

The parts of boundaries obtained by the hierarchical convexity rule correspond for many objects to the parts obtained using points of minimal negative curvature. This is illustrated in Fig. 5, which presents (after the arrows) all possible codon quadruples scanned from Fig. 7 in Hoffman and Richards [12]. Shapes simplified by our discrete curve evolution are presented before the arrows. The endpoints of maximal convex arcs determined on the simplified shapes are marked by small circles. For the original shapes in Fig. 5, the endpoints of the maximal convex arcs are located near the points of minimal negative curvature. This is also the case for the shapes in Fig. 4.

In our approach, we do not need to decide which points of minimal negative curvature have to be joined together in order to obtain object parts. The object parts obtained by joining two negative curvature minima are called *part cuts* (Beusmans *et al.* [5]). As argumented in Hoffman and Singh [13], a separate theory is necessary to determine the part cuts knowing the boundary points of minimal negative curvature.

- In our approach, the part cuts are automatically determined by maximal convex arcs.

We simply obtain part cuts by joining the endpoints of maximal convex arcs on the original shape. Observe that the endpoints do not have to be direct neighbors on the original contour; e.g., see the part cut that determines the upper body of the bear in Fig. 4c.

Also, for many objects, the obtained parts of objects correspond to limbs and necks in the theory of Siddiqi and Kimia [25].

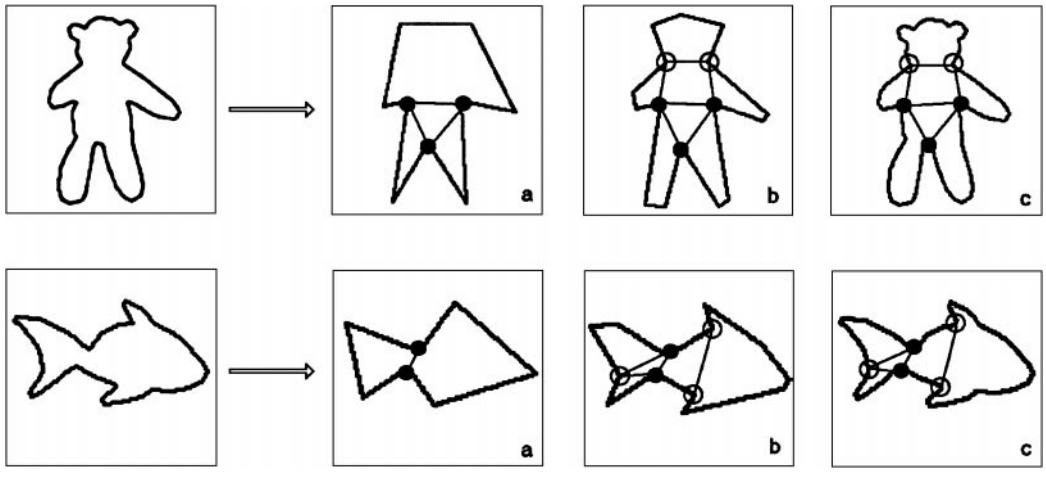

FIG. 4. The object parts obtained at different levels of the discrete evolution of the boundary curve.

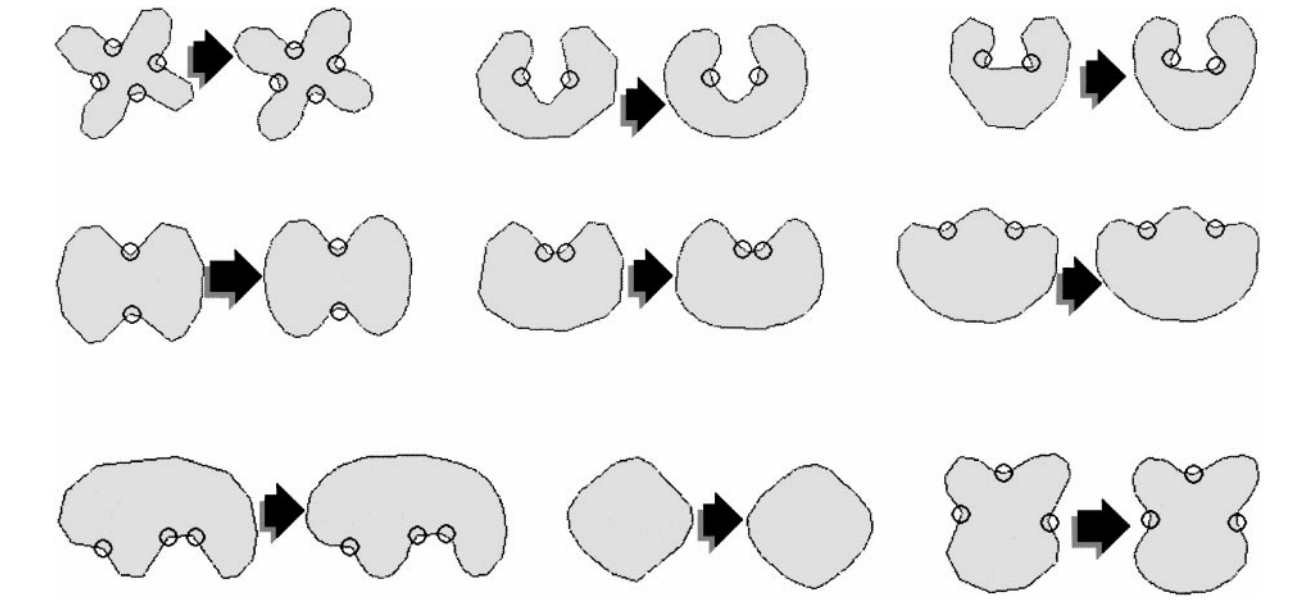

FIG. 5. The endpoints of maximal convex arcs correspond to points of minimal negative curvature. The shapes after the arrows are scanned from Hoffman and Richards [12].

For example, the parts obtained by the hierarchical convexity rule include mostly limbs and necks in the theory of Siddiqi and Kimia for the shapes in Fig. 6, which presents some of the shapes used in Siddiqi *et al.* [27] for psychological experiments to justify limbs and necks. For every shape, three stages of its evolution together with the parts obtained at these stages are shown. The parts obtained by the hierarchical convexity rule are marked on the original shape by different gray-level values. The darker the gray-level value, the higher is the level of the evolution at which a part is determined. A part contains all regions that have darker gray-level values, e.g., the part "fish tail" (marked light gray) contains the two black "fish tail tip" regions.

Observe that the parts obtained by our rule include all parts with a high degree of intersubject consistency obtained by psychological experiments in [27] (Fig. 17); e.g., these are the front leg and the ear for the donkey, the tail and the fins for the fish, and the front leg for the rabbit. For the kangaroo, no such parts were determined in [27]. Most of the remaining parts in Fig. 6 determined by our rule correspond also to the parts determined by the subjects in experiments in [27] (which have a low degree of intersubject consistency). This is, for example, the front part of the donkey determined by the vertical part-line. This visual part illustrates an additional strength of our approach, since it seems to be plausible and has been identified by the experiments in [27]. However, this visual part can be obtained neither by the codon theory in [12] nor by the theory in [25].

The hierarchy obtained by the evolution of a boundary curve induces a hierarchical structure of the visual parts, which we will call *shape hierarchy*:

- The more advanced is the process of the evolution, the more significant for the object shape are the parts determined.
- The parts obtained on a higher level of the shape hierarchy are inherited to the lower levels.

This means that on a lower level only the inherited parts are further divided. For example, on the level (b) in Fig. 4, only the parts obtained on level (a) are further divided; e.g., the upper body of the bear is divided into the head and arms. For the rabbit in Fig. 8, we have the following shape hierarchy of visual parts: (f) > (e) > (d).

Our shape hierarchy corresponds to the hierarchy of parts based on the evolution of shocks in the entropy scale space in Kimia *et al.* [14]. As argumented in [14], the evolution of shocks requires not only boundary, but also region information. However, observe that our part decomposition requires only boundary information. This means that our approach to shape decomposition allows us to obtain the region information from the evolution hierarchy of the boundary curve. This is the case for a large class of shapes, e.g., the tail of the fish in Fig. 6, but there exist shapes for which our boundary information and evolution hierarchy do not determine the region information, e.g., the two ears of the rabbit in Fig. 6 are not identified as a visual part; surprisingly, this part is also not identified as a visual part in psychological experiments in [27]. However, for the worm shape in Fig. 5 in [27], our algorithm might give parts that are not intuitive due to the lack of explicit region information.

For boundaries of continuous objects, the endpoints of maximal convex arcs correspond to inflection points (e.g., inflection points are used for shape description in Freeman [6]). The correspondence of the endpoints of maximal convex arcs to different kinds of critical points (in the sense of differential geometry) is possible, since we work in a discrete space which does not exactly follow the rules of differential geometry.

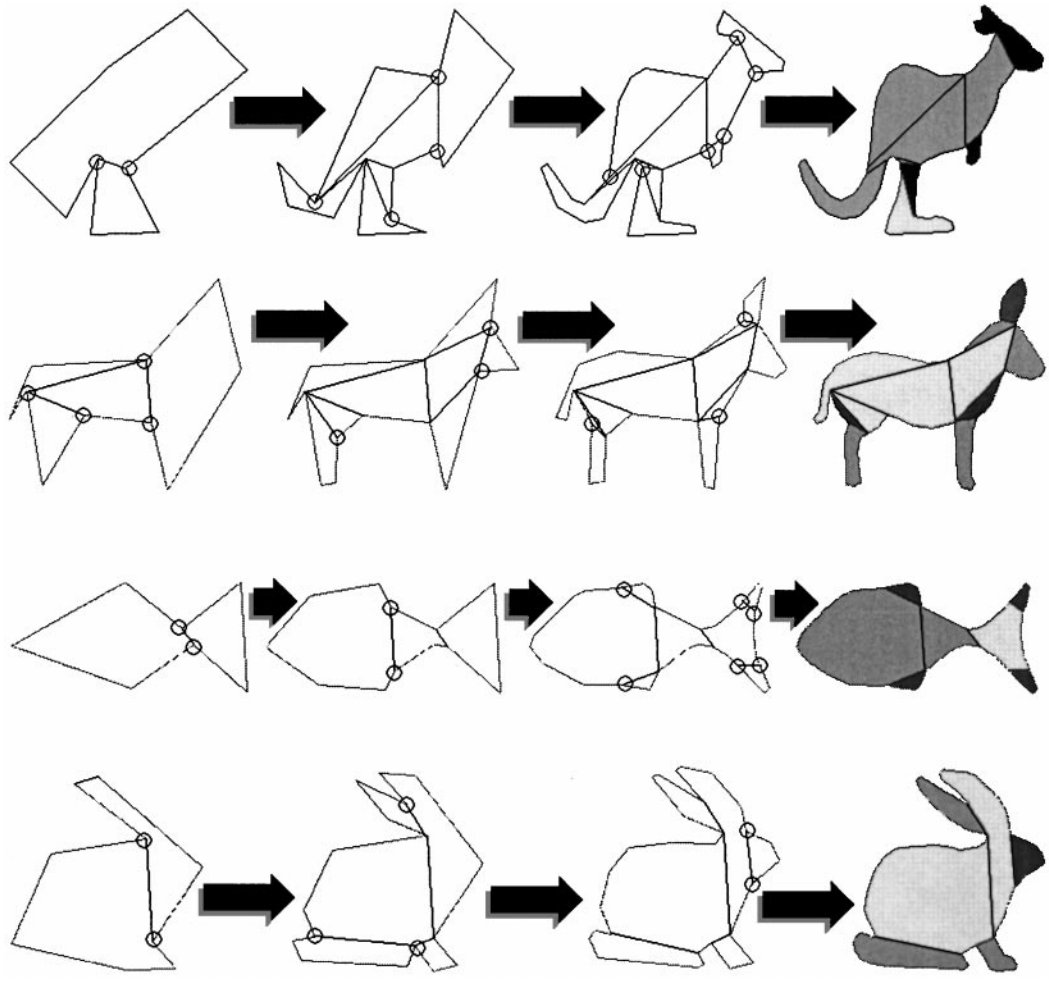

FIG. 6. For these shapes, the parts obtained by the hierarchical convexity rule include most of the limbs and necks in the theory of Siddiqi and Kimia. The shapes are scanned from [27].

Our approach allows us additionally

- to obtain a shape decomposition stable with respect to noise, due to properties of our discrete curve evolution and due to the fact that the convex arcs represent global properties of object boundaries,
- to give a relevance measure for obtained parts that is based on the level of the shape hierarchy and on relevance of the maximal convex arcs.

The stability of the shape decomposition with respect to noise results from the fact that our evolution process is guided by the relevance order (described in more details in Section 3) and due to the fact that recognition of supported arcs is based on global features that are significantly less influenced by noise than locally defined points of minimal negative curvature. The stability is demonstrated in Fig. 7. Although the original contour of the fish is distorted by two different levels of noise, the obtained parts are the same as for the original fish in Fig. 4.

In our approach, we can derive a relevance measure of visual parts from the relevance measure of supported arcs; i.e., the relevance measure of visual parts is based on the relevance of the contribution of the maximal convex arcs by which they are determined to the object shape, which depends on the total turn (i.e., global curvature) and the length that is normalized with respect to the total length of the boundary curve (see Section 4). Additionally, the relevance measure of visual parts is based on the levels of the shape hierarchy on which they are determined, similarly to the case in Kimia *et al.* [14] (see also [25]). Thus, we can obtain a relevance measure together with object parts. In contrast, part decomposition based on points of minimal negative curvature is binary; i.e., the obtained parts cannot be distinguished according to their salience.

3. DISCRETE CURVE EVOLUTION BY LINEARIZATION

The presented discrete curve evolution method by linearization has been applied to digital simple closed 8-curves. We have used a watershed segmentation algorithm that automatically produces such curves as boundary curves of digital objects in real

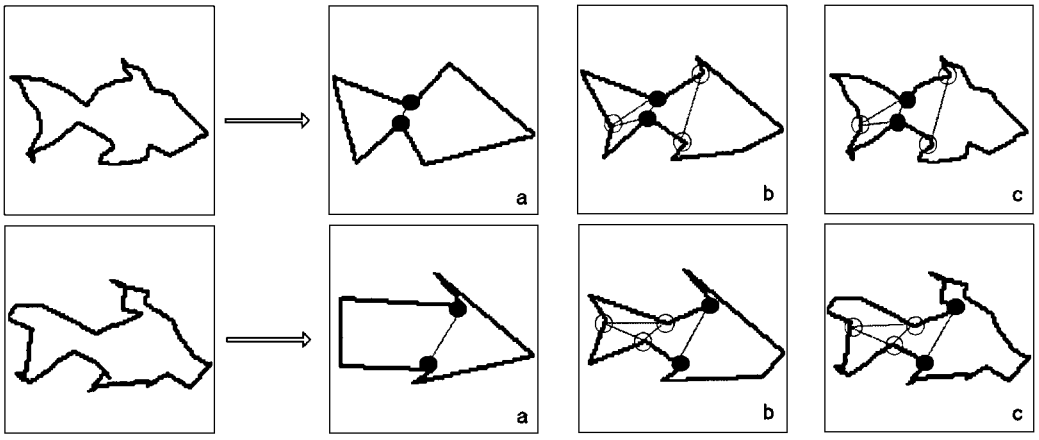

FIG. 7. The proposed decomposition into visual parts is stable with respect to contour distortions.

images.[1] Therefore, our discrete curve evolution as well as the shape decomposition algorithms can be applied to real images. This is demonstrated in Fig. 8.

First the original image (Fig. 8a) is segmented using color and texture segmentation as in Pauwels *et al.* [24]. The watershed algorithm produces the object contour (Fig. 8c) that is a simple closed 8-curve. In Figs. 8d–8f, we see a few stages of the discrete curve evolution. The obtained evolution hierarchy (8f) > (8e) > (8d) yields the illustrated decomposition into visual parts.

In the first step of our discrete curve evolution method, a digital curve is divided into maximal digital line segments. The decomposition of a digital curve into maximal line segments is based on the observation that every digital curve can be decomposed into digital line segments, even if the curve is strongly distorted by noise. We use a linear algorithm (with respect to the number of points in the curve) from Debled and Reveilles [8] to obtain a decomposition of a digital curve into maximal digital line segments. The decomposition in linear time belongs to newer achievements of digital geometry; a first linear algorithm was given 1991 by Smeulders and Dorst [28].

The process of *discrete curve evolution by digital linearization* is very simple:

- The minimum of the cost function K (defined in Section 4) determines the pair of line segments that is substituted by a single line segment joining their endpoints. The substitution determines a single step of the discrete curve evolution. We repeat this process for the new curve; i.e., we determine again the pair of line segments that minimizes the cost function, and so on.

Let $\mathcal{D}_m = s_0, \ldots, s_{m-1}$ be a decomposition of a digital curve C into consecutive digital line segments. The algorithm that computes the decompositions $\mathcal{D}_k$ for each stage of the discrete curve evolution $k > 3$ until $\mathcal{D}_{k-1}$ is convex is the following:

Discrete Curve Evolution Procedure($\mathcal{D}_m$)
k = m;
Do
  Find in $\mathcal{D}_k$ a pair s_i, s_{i+1} (mod k) such that $K(s_i, s_{i+1})$ is minimal;
  $\mathcal{D}_{k-1} = \mathcal{D}_k$ with segments s_i, s_{i+1} replaced by line segment s' that joints the endpoints of arc $s_i \cup s_{i+1}$;
  k = k − 1;
until $\mathcal{D}_{k-1}$ is convex.

This algorithm is guaranteed to terminate, since in every evolution step, the number of digital line segments in the curve decomposition decreases by one (one line segment replaces two

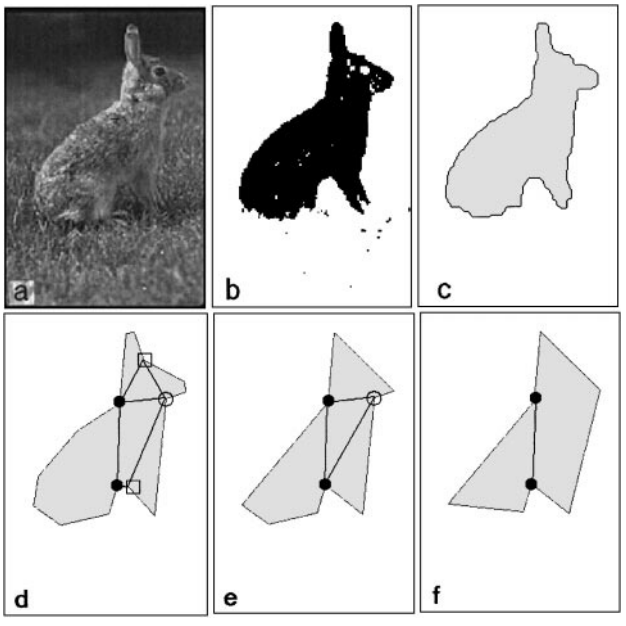

FIG. 8. From an image to a simplified shape representation and to visual parts. (a) → (b), color and texture segmentation (Pauwels *et al.*); (b) → (c), watershed segmentation; (c)–(f), discrete curve evolution and obtained visual parts.

[1] This watershed algorithm was successfully applied in image segmentation for object based data representation of video sequences, see Lakämper and Seytter [16].

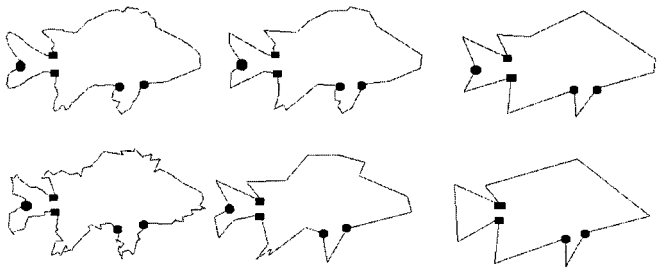

FIG. 9. The unchanged planar position of the points marked with the same symbols demonstrates that there is no displacement of the remaining feature points.

adjacent segments). It is also obvious that this evolution converges to a convex polygon, since the evolution will reach a state where there are exactly three line segments in the curve decomposition, which clearly form a triangle. Of course, for many curves, a convex polygon with more then three sides can be obtained in an earlier stage of the evolution. Thus, we obtain

PROPOSITION 1. *Discrete curve evolution by digital linearization converges to a convex polygon.*

This proposition demonstrates the mathematical simplicity of the relation between our evolution approach and the geometric properties of the obtained digital curves. Observe that we did not assume that the digital curve is simple (i.e., has no self-intersections). An analog theorem for the evolution of continuous planar curves by diffusion equations is a deep and highly nontrivial result of differential geometry (Grayson [7]). It holds only for simple closed smooth curves evolved by diffusion equations.

Polygonal analogs of the evolution by diffusion equations are presented in Bruckstein *et al.* [3]. The experiments in [3] indicate that an arbitrary initial polygon converges to a convex polygon (polygonal circle). However, the proof of this fact in the Euclidean case is an open question. In [3] as well as in evolutions by numerical solutions of differential equations, each vertex of the polygon is mapped to some point in the plane at a single evolution step, whereas in our approach one vertex is removed and the remaining vertices do not change their positions. This is an important difference in favor of our approach.

Now we list some important properties of our discrete curve evolution:

(P_1) It leads to the simplification of shape complexity, in analogy to evolutions guided by diffusion equations, with

(P_2) no blurring (i.e., shape rounding) effects and no dislocation of relevant features,

due to the fact that the remaining vertices do not change their positions. Two more important properties of our discrete curve evolution are based on the relevance measure K (defined in Section 6):

(P_3) It is stable with respect to noisy deformations, since noise elimination takes place in the early stages of the evolution.

(P_4) It allows us to find digital line segments in noisy images, due to the relevance order of the repeated process of digital linearization (e.g., Fig. 10).

We begin with some examples to illustrate the properties of our evolution method. A few stages of the proposed discrete curve evolution in Fig. 1 illustrate the shape complexity reduction (P_1) of the original curve (a). Our discrete curve evolution does not introduce any blurring effects (P_2), which result in shape rounding for curves. For a comparison see the discrete curve evolution on the WWW page http://www.ee.surrey.ac.uk/Research/VSSP/imagedb/demo.html, based on [22]. Observe also that there is no dislocation of the remaining relevant shape features (P_2), since the planar position of the remaining points of the digital polygon is unchanged. The stability of relevant shape feature points is demonstrated by marking the corresponding points with the same symbols in Fig. 9. Observe also the stability of feature points with respect to noise deformations shown in the second row in Fig. 9.

By comparison of the curves (a) and (b) in Fig. 10, it can be seen that our evolution method allows us first to eliminate noise influence without changing the shape of objects (P_3). If we continue to evolve the curve (b), we obtain line segments that are relevant to the curve shape (P_4) in (c); cf. Brunn *et al.* [4], Fig. 4.

Our evolution method allows us to eliminate noise influence without changing the shape of objects (P_3), since distortions caused by noise mostly result in pairs of digital line segments that have relatively low values of the relevance measure K (presented in Section 4): The relevance order induced by K begins with pairs of arcs that contribute in the least significant way to the shape of a given curve, which are arcs of relatively small length

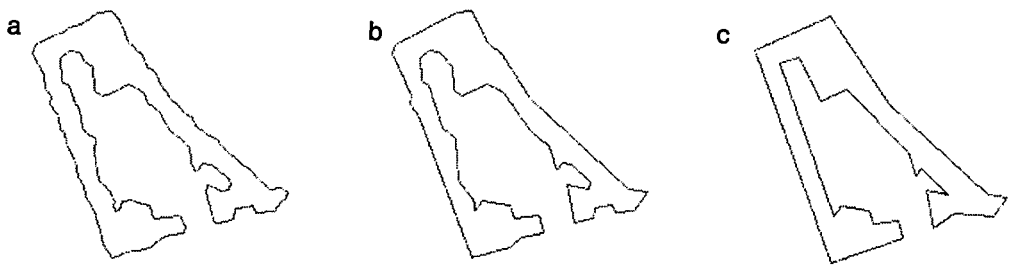

FIG. 10. (a) → (b), noise elimination; (b) → (c), extraction of relevant line segments.

and total curvature. Such arcs are most likely to result from noise distortions. Since they are removed in the early stages of the discrete curve evolution, the results of the presented evolution are very stable with respect to noise. For example, although the boundary curves (2a) and (3a) in Fig. 16 are distorted by noise to a large extent in various ways, the results of the evolution of curves in (1a), (2a), and (3a) are very similar. The robustness of our discrete curve evolution method with respect to noise is also due to the fact that we are using global curvature information. A more formal justification of the above properties can be found in [18].

4. RELEVANCE ORDER

Our evolution process is guided by a relevance order. We assign to every pair of two adjacent line segments s_1, s_2 in a decomposition of a given digital curve C a cost $K(s_1, s_2)$ which represents the significance of the contribution of arc $s_1 \cup s_2$ to the shape of C. We order pairs of adjacent line segments with respect to this significance cost. We will call this order a *relevance order*. The exact value of the cost function we used in our experiments is given by the formula (1) in Section 6 and can be interpreted as a linearization cost of arc $s_1 \cup s_2$. To motivate and derive this formula, we use a tangent space representation of digital curves in Sections 5 and 6. In this section, we state basic requirements for the relevance order.

The linearization cost $K(a)$ of any supported arc a depends on its relative length (with respect to the curve) and its global curvature. (In particular, a pair of two adjacent line segments s_1, s_2 forms a supported arc $s_1 \cup s_2$.)

It seems that an adequate measure of the relevance of arc $s_1 \cup s_2$ for the shape of a given object can be based on turn angle $\beta(s_1, s_2)$ and on the relative lengths of the segments $l(s_1), l(s_2)$. We assume that the larger both relative lengths and the total turn of the arc, the greater is its contribution to the shape of a curve. Thus, the cost function K is monotonically increasing with respect to the relative lengths and the total curvature. This assumption can be justified by the rules on the salience of a limb in Siddiqi and Kimia [25]. It can be also motivated by the example objects in Fig. 11 and by the experimental results

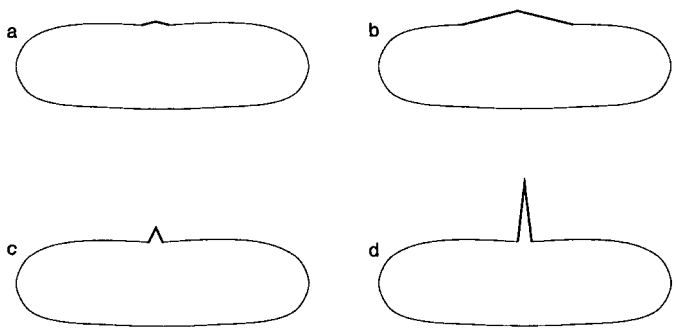

FIG. 11. The influence of the bold arcs on the shape of the curve depends on their turn and length of their segments.

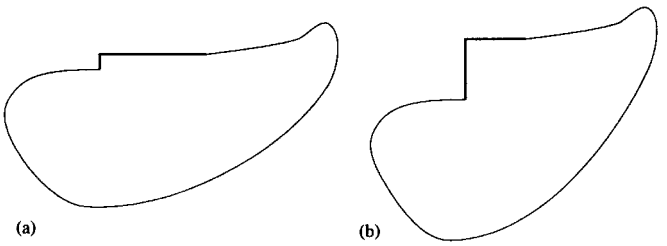

FIG. 12. Although the two bold arcs have the same total length, the significance of their contribution to the shape of the curves is different.

described below. The bold arc in Fig. 11b has the same turn as the bold arc in Fig. 11a but is longer, and the bold arc in Fig. 11c has the same length as the bold arc in Fig. 11a but its turn is greater. While the bold arc in Fig. 11a can be interpreted as an irrelevant shape distortion, the bold arcs in Figs. 11b and 11c are more likely to represent relevant shape properties of the whole object. As can be easily observed, the contribution of the bold arc in Fig. 11d to the shape of the displayed object is the most significant. This arc has the largest turn and its line segments are longer than in Figs. 11a and 11c. Although the line segments of bold arcs in Figs. 11b and 11d have the same length, the shape contribution of the bold arc in Fig. 11d is clearly more significant than the contribution of the bold arc in Fig. 11b due to the difference in turn angle.

Observe that the total relative length of the line segments $(l(s_1) + l(s_2))$ is not appropriate as a parameter for the cost function K. The total length of the bold arcs in Fig. 12 is the same, but it can be easily seen that the contribution to the shape of the whole curve of the arc in Fig. 12b is more significant than the contribution of the arc in Fig. 12d.

The example in Fig. 12 may suggest that the cost function $K(s_1, s_2)$ should be directly proportional to the area of the region enclosed by $s_1 \cup s_2$, since the area is greater for the bold arc in Fig. 12b. However, this is not the case, as can be seen by comparing the two bold arcs in Figs. 11b and 11d. It can be clearly seen that the significance of the contribution of the bold arc to the shape of the contour in Fig. 11d is larger than in Fig. 11b, but the area of the triangular region enclosed by the bold arc in Fig. 11d is smaller than that in Fig. 11b (the line segments of the two bold arcs have the same length).

5. TANGENT SPACE REPRESENTATION

To derive the formula for the relevance measure, we use a *tangent space* in which a step function is associated with every digital curve.

Any digital curve C can be interpreted as a polygonal curve with a possibly large number of vertices. For example, all points on the digital curve can be the vertices or the vertices can be chosen to be the endpoints of the maximal digital line segments contained in C. Thus, we assume that digital curve C is a polygonal curve with vertices $v_0, \ldots, v_{m-1}$. Hence C is composed of digital line segments $\mathcal{D}_m(C) = s_0, \ldots, s_{m-1}$, where s_i is the

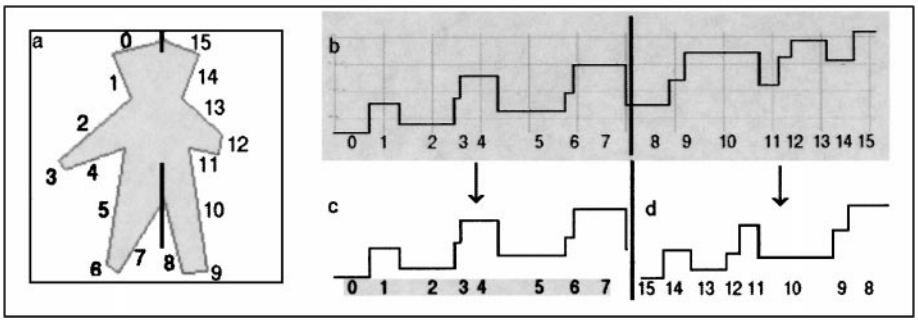

FIG. 13. A polygonal curve (a) and its step function representation in the tangent space (b). The similarity of (c) and (d) shows that the curve (a) is symmetric.

(continuous) line segment joining v_i to v_{i+1} for $i = 0, \ldots, m-1$ modulo $m-1$. We denote *angle*(s) to be the angular direction of line segment s in the standard coordinate system of the plane and we denote $l(s)$ to be the length of s normalized by the length of C.

A polygonal curve is represented in the tangent space by the graph of a step function, where the x-axis represents the arclength coordinates of points in C and the y-axis represents the direction of the line segments in the decomposition of C. For example, Fig. 13 shows a digital curve (a) and its step function representation (b) in the tangent space. Formally, the *tangent space* is a torus $S_1 \times S_2$, where S_1 is a circle of length one that represents the length of a digital curve and S_2 is a circle that represents the angular direction of digital line segments. We will display the tangent space as a rectangle with the parallel sides identified in the standard way to obtain a topological torus. The y-difference between two adjacent steps in the tangent space represents the turn angle of the corresponding pair of line segments. The significance of the contribution of a pair of consecutive line segments to the shape depends on their length and the turn angle in the direction of traverse. Exactly these two parameters are represented in the tangent space.

We define a transformation T mapping a digital 8-curve to the tangent space. For illustration, see Figs. 13(a) and 13(b). To each digital line segment $s \in \mathcal{D}_m(C)$, a line segment $T(s)$ in the tangent space is assigned such that

$$\pi_y(T(s)) = angle(s),$$

the length of $\pi_x(T(s))$ is equal to $l(s)$, and $\pi_x(T(s_i))$ is adjacent to $\pi_x(T(s_{i+1}))$, where π_x and π_y denote the projections on x- and y-axes in the tangent space, correspondingly. This means that the y-values of all points in $T(s)$ are equal to *angle*(s) and the projection of $T(s)$ on the x-axis has the same (normalized) arclength coordinates as s in C.

An analytical description of the transformation to the tangent space for continuous curves can be found in Zahn and Roskies [33]. They call the step function in the tangent space a *cumulative angular bend function*. Zahn and Roskies use this transformation only as an intermediate step to obtain Fourier descriptions of planar curves. They use the tangent space neither for analyzing the underlying planar curves nor for scale transformations, which we will describe below. Uesaka [30] uses the transformation of polygonal arcs to the tangent space to determine a circular approximation of polygonal arcs.

6. RELEVANCE MEASURE

For each two adjacent line segments s_1, s_2 in the decomposition of a digital curve C, we determine the relevance measure $K(s_1, s_2)$, which represents the significance of the contribution of arc $s_1 \cup s_2$ to the shape of C. The value $K(s_1, s_2)$ can be interpreted as the cost required for linearization of arc $s_1 \cup s_2$.

Let $s_1 = AB$ and $s_2 = EF$ be two consecutive line segments in the decomposition of curve C, so that $B = E$ is their common endpoint (see Fig. 14) and $\beta = \beta(s_1, s_2)$ is the turn angle, i.e., $angle(EF) - angle(AB) = \beta$ (where *angle*(s) represents the angular direction of line segment s). We determine the circular arclength by which the endpoints B and F must be rotated

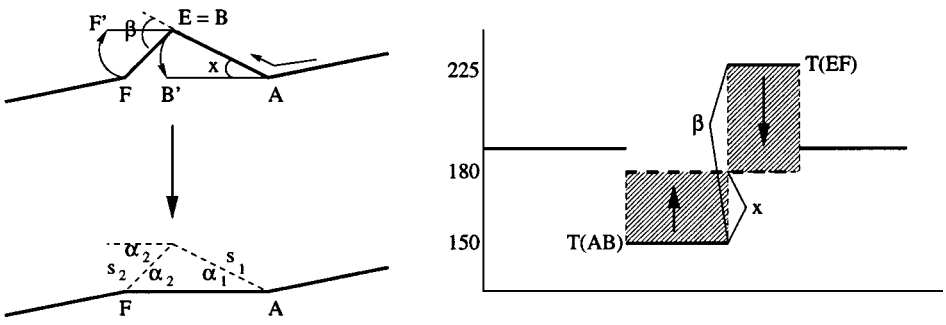

FIG. 14. Scale transformation in the tangent space.

around points A and E, correspondingly, so that the rotated line segments have the same direction, i.e., until AB' and EF' are parallel, where B' and F' are the images of B and F by the rotations. The circular arclength must be equal for both line segments. The cost function K assigns to pair s_1, s_2 this circular arclength. We will show below that it is given by the equation

$$K(s_1, s_2) = \frac{\beta(s_1, s_2) l(s_1) l(s_2)}{l(s_1) + l(s_2)}, \tag{1}$$

where l is the length function normalized with respect to C.

Without loss of generality, we can assume that $angle(EF) - angle(AB) = \beta > 0$. We seek an angle x, $0 \le x \le \beta$ such that

$$angle(s_1) + x = angle(s_1) - (\beta - x) \tag{2}$$

and

$$l(s_1)x = l(s_2)(\beta - x). \tag{3}$$

Equation (2) expresses that line segments s_1 and s_2 have the same angular direction after the rotations. Equation (3) expresses that their endpoints must be rotated by the same circular arclength. The pair of equations (2) and (3) can be interpreted in the tangent space (see Fig. 14 (right)) as translation of steps $T(s_1)$ and $T(s_2)$ parallel to the y-axis until they have the same (angular) y-value and the rectangles obtained by their moves have the same area. By simple calculation, we obtain $x = \beta l(s_2)/[l(s_1) + l(s_2)]$, and consequently, by (3), the circular arclength is equal to (1).

The cost function in (1) is our measure of how significant is the contribution of a pair of consecutive line segment to the shape of the curve. The minimum of the cost function determines the pair that is substituted by a single line segment joining their endpoints, which results in a single step of discrete curve evolution, e.g., if K obtains the minimum for line segments AB and EF, then they are deleted from C and the new line segment AF is added to C. The result of substituting the segments AB and EF with segment AF is shown in Fig. 14 (left).

The tangent space representation is transformed in the corresponding way (see Fig. 14 (right)): the steps $T(AB)$ and $T(EF)$ are deleted and a new step $T(AF)$ is added. Since it is not sufficient to represent the length of the new step $T(AF)$ by $l(s_1) + l(s_2)$, we take the length of digital segment AF as the length of step $T(AF)$, i.e., the length of $T(AF)$ is equal to

$$l_{AF} = \sqrt{l(s_1)^2 + l(s_2)^2 + 2l(s_1)l(s_2)\cos\beta}.$$

Examples of the discrete curve evolutions together with the corresponding transformations of the tangent spaces are shown in Figs. 17 and 18.

The value (1) of the cost function determines the rotations of line segments s_1 and s_2 until they are parallel. In the process of discrete curve evolution, the segments s_1 and s_2 are substituted by a line segment s' joining the endpoints of $s_1 \cup s_2$. In the following, we show that the rotations yield an equivalent change of curve C as substitution of segments s_1 and s_2 by s' if the rotations angles are *small*. This also justifies the interpretation of $K(s_1, s_2)$ as the cost required for linearization of arc $s_1 \cup s_2$.

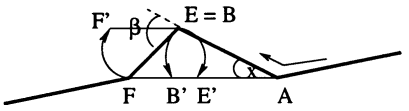

FIG. 15. The rotated segments AB' and FE' must be contained in $s' = AF$ if the rotations angles are *small*.

We recall that $s_1 = AB$ and $s_2 = EF$ are two consecutive line segments in the decomposition of curve C, such that $B = E$ is their common endpoint (see Fig. 14). We rotated segment EF around point E so that the length of circular arc FF' is given by Eq. (1). Now we change the interpretation of this rotation (see Fig. 15): we rotate EF around point F so that the length of arc drawn by E is given by Eq. (1), i.e., circular arc EE' is given by Eq. (1). We will show below that the rotated segments AB' and FE' must be contained in $s' = AF$ if the rotations angles are *small*.

Precisely, we will show that the segments obtained by the rotation of AB and EF around points A and F, correspondingly, are located *very close* to AF if angles $\alpha_1 = BAF$ and $\alpha_2 = EFA$ are *small* (see Fig. 15).

Small means here that $\sin(\alpha_1) \approx \alpha_1$ and $\sin(\alpha_2) \approx \alpha_2$, which is usually assumed for angles less than some γ in the interval $[\frac{\pi}{12}, \frac{\pi}{9}]$, depending on the required accuracy.

Since the rotation angle of a line segment around one of its endpoints is the ratio of the circular arc length drawn by the other endpoint during the rotation to the length of the segment, we obtain from Eq. (1) that the rotation angles for segments AB and EF are

$$x = w_1 = \frac{\beta l(s_2)}{l(s_1) + l(s_2)} \quad \text{and} \quad w_2 = \frac{\beta l(s_1)}{l(s_1) + l(s_2)}.$$

By the sinus formula

$$\frac{l(s_1)}{\sin\alpha_2} = \frac{l(s_2)}{\sin\alpha_1}, \quad \text{we have} \quad \frac{l(s_1)}{\alpha_2} \approx \frac{l(s_2)}{\alpha_1}.$$

Since $\beta = \alpha_1 + \alpha_2$, it can be easily calculated that

$$\frac{\beta l(s_2)}{l(s_1) + l(s_2)} \approx \alpha_1 \quad \text{and} \quad \frac{\beta l(s_1)}{l(s_1) + l(s_2)} \approx \alpha_2,$$

which implies that

$$w_1 \approx \alpha_1 \quad \text{and} \quad w_2 \approx \alpha_2.$$

This means that segments AB and EF after rotation by angles w_1 and w_2 around points A and F, correspondingly, will be nearly contained in the segment AF. Since we deal with digital segments, the approximation accuracy can be calculated with respect to resolution of the square grid. We will not discuss this subject here; it is related to the sufficient digitization resolution (see Gross and Latecki [10]).

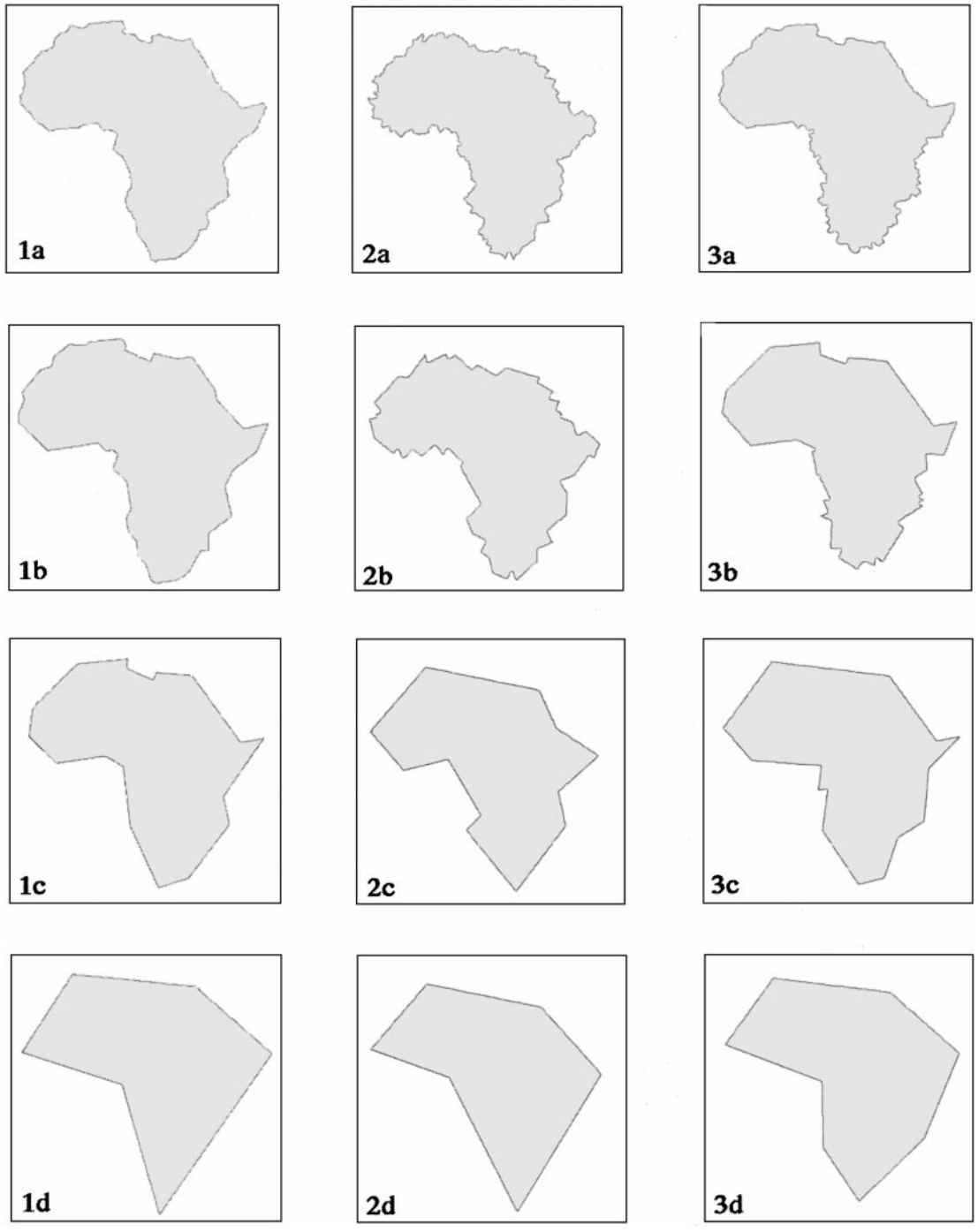

FIG. 16. Shape evolution by repetitive linearization. Compare to the diffusion based evolution of similar contours in Mokhtarian and Mackworth [22].

Since the values of the cost function can be defined in the tangent space, which is a torus, the presented evolution method is rotation invariant. Since the curve length is normalized, the evolution is scaling invariant. Since the minimum of the cost function does not depend on the direction and order of the traversal of line segments, the evolution is reflection invariant. It can be easily seen that it is also translation invariant.

7. CONCLUSIONS AND FUTURE WORK

Since contours of objects in digital images are distorted due to digitization noise and due to segmentation errors, it is desirable to neglect the distortions while at the same time preserving the perceptual appearance at a level sufficient for object recognition. An obvious way to neglect the distortions is to eliminate

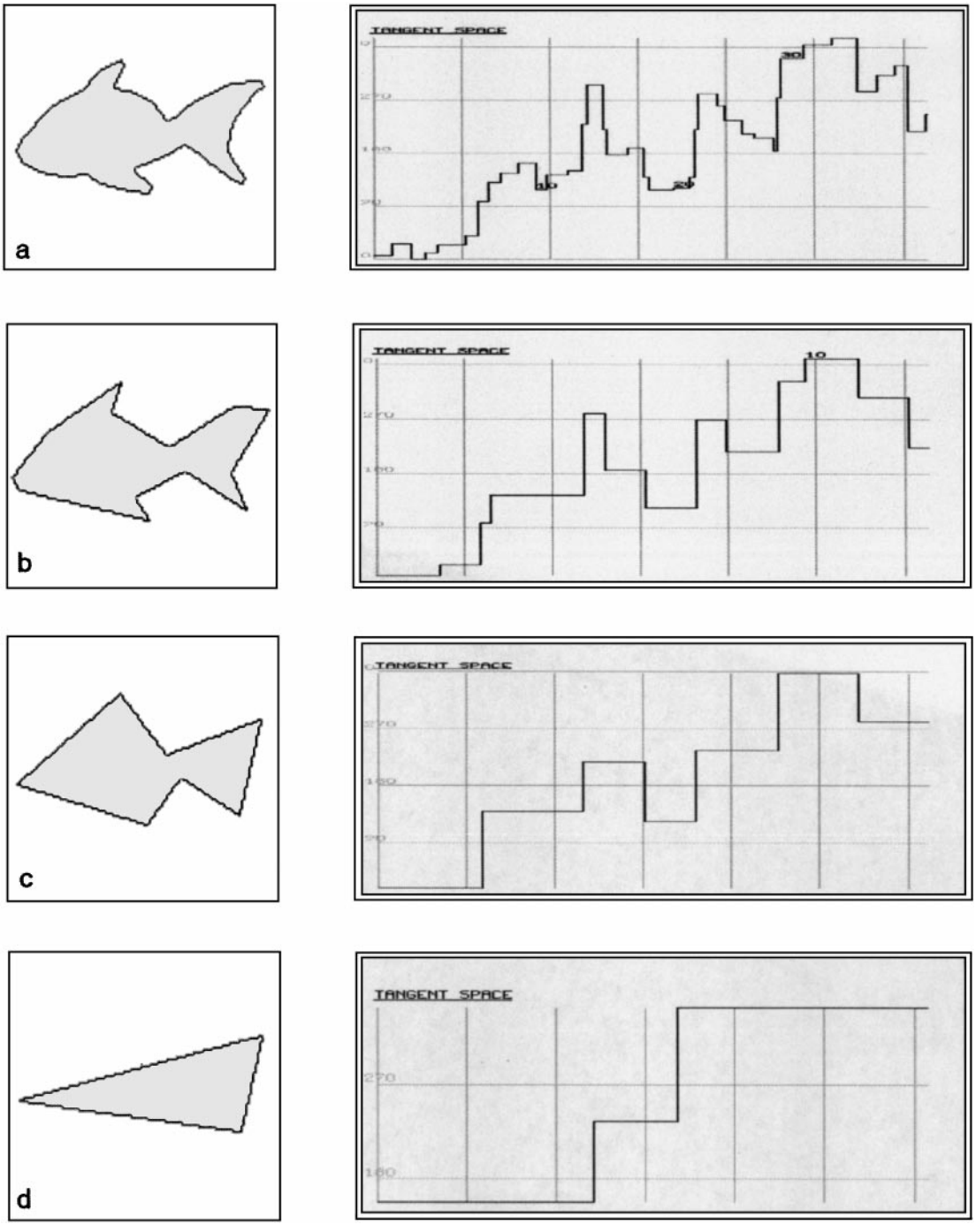

FIG. 17. Shape evolution by repetitive linearization. Next to each curve is its tangent space representation.

them by approximating the original contour with one that has a similar perceptual appearance. To achieve this, an appropriate approximation (or discrete curve evolution) method is necessary. This is achieved in our approach through a novel method for evolution of polygonal curves (which can also be interpreted as an approximation method). For this method, we can determine a universal stage of the discrete curve evolution (that does not depend on a given shape and on the amount of the distortions) at which the distortions are eliminated and the perceptual appearance is sufficient for robust object recognition. This is an important feature of our discrete curve evolution method, since it implies that neglecting the distortions is achieved automatically, which is a necessary requirement for shape representations used in image databases. Observe that no universal solutions exist to determine such a stage for many established methods, e.g., to determine the approximation distance for a popular contour

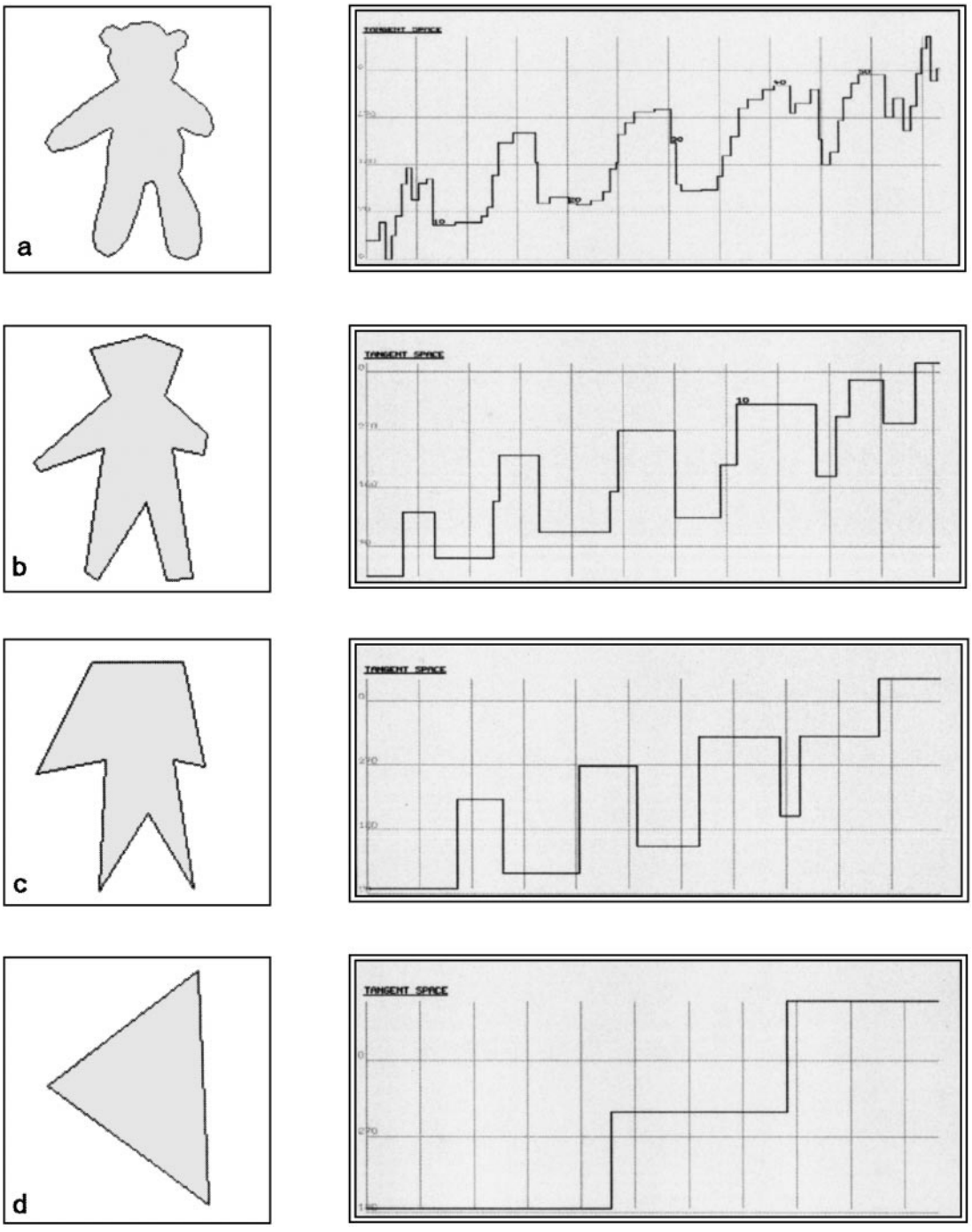

FIG. 18. Shape evolution by repetitive linearization. Next to each curve is its tangent space representation.

approximation method [23] by Ramer, for multiscale contour approximation [2] by Bengtsson and Eklundh, and for curvature scale filtering, e.g. [32], where a few multiscale parameters are necessary.

The presented tangent space allows us to reduce the complexity of symmetry detection in the presence of noise and occlusions, which is a complicated task (see, e.g., Tek *et al.* [29]). The symmetry of some boundary parts of a given object can be detected given the step function representations of the boundary curve: If boundary part A is a symmetric image of part B, then the step function of A is equal to the point reflection of the step function of B. For example, the point reflection of part 8–15 of the step function in Fig. 13(b), shown in (d), is equal to part 0–7, shown in (c).

The hierarchical shape decomposition into visual parts and shape simplification by discrete curve evolution make it possible

to define a similarity measure for planar objects. This measure is defined and applied for automatic object indexing and search in image databases in [19]; see also our web side [20]. The fact that the performance of our similarity measure is in accord with our visual perception justifies perceptual adequacy and usefulness of the presented discrete curve evolution and the shape decomposition methods.

These topics as well as a 3D version of our results will be treated in forthcoming papers. While our 2D evolution by digital linearization is length-minimizing, the 3D analog is area-minimizing.

ACKNOWLEDGMENTS

The work of Longin Jan Latecki was supported by Project Ec 170/1-1 of the German Research Foundation (DFG). We greatly appreciate the help of Professor Ulrich Eckhardt (Institut für Angewandte Mathematik, Universität Hamburg) and Professor Hans-Joachim Kroll (Mathematisches Institut, Technische Universität München), who made this project feasible. We also appreciate helpful comments and advice from Professor Ulrich Eckhardt and Professor Kaleem Siddiqi.

REFERENCES

1. R. Basri, L. Costa, D. Geiger, and D. Jacobs, Determining the similarity of deformable shapes, *Vision Res.*, to appear.
2. A. Bengtsson and J.-O. Eklundh, Shape representation by multiscale contour approximation, *IEEE Trans. Pattern Anal. Mach. Intell.* **13**, 1991, 85–93.
3. A. M. Bruckstein, G. Shapiro, and C. Shaked, Evolutions of planer polygons, *Int. J. Pattern Recog. Artificial Intell.* **9**, 1995, 991–1014.
4. A. Brunn, U. Weidner, and W. Förstner, Model-based 2D-shape recovery, in *Proc. of 17th DAGM Conf. on Pattern Recognition (Mustererkennung), Bielefeld*, pp. 260–268, Springer-Verlag, Berlin, 1995.
5. J. Beusmans, D. D. Hoffman, and B. M. Bennett, Description of solid shape and its inference from occluding contours, *J. Opt. Soc. Am. A* **4**, 1987, 1155–1167.
6. H. Freeman, Shape description via the use of critical points, *Pattern Recog.* **10**, 1978, 159–166.
7. M. A. Grayson, The heat equation shrinks embedded plane curves to round points, *J. Differential Geom.* **26**, 1987, 285–314.
8. I. Debled-Rennesson and J.-P. Reveilles, A linear algorithm for segmentation of digital curves, *Int. J. Pattern Recog. Artificial Intell.* **9**, 1995, 635–662.
9. G. Dudek and J. K. Tsotsos, Shape representation and recognition from multiscale curvature, *Comput. Vision Image Understanding* **68**, 1997, 170–189.
10. A. Gross and L. Latecki, Digitizations preserving topological and differential geometric properties, *Comput. Vision Image Understanding* **62**, 1995, 370–381.
11. A. Gross and L. J. Latecki, A realistic digitization model of straight lines, *Comput. Vision Image Understanding* **67**, 1997, 131–142.
12. D. D. Hoffman and W. A. Richards, Parts of recognition, *Cognition* **18**, 1984, 65–96.
13. D. D. Hoffman and M. Singh, Salience of visual parts, *Cognition* **63**, 1997, 29–78.
14. B. B. Kimia, A. R. Tannenbaum, and S. W. Zucker, Shapes, shocks, and deformations, I: The components of shape and the reaction–diffusion space, *Int. J. Comput. Vision* **15**(3), 1995, 189–224.
15. J. J. Koenderink and A. J. Doorn, The shape of smooth objects and the way contours end, *Perception* **11**, 1981, 129–137.
16. R. Lakämper and F. Seytter, Manipulation objektbasiert codierter Bilder als Anwendungsbeipspiel neuer Videostandards, in *Proc. of 19th DAGM Conf. on Pattern Recognition (Mustererkennung), Braunschweig*, pp. 427–434, Springer-Verlag, Berlin/New York, 1997.
17. L. J. Latecki and A. Rosenfeld, Supportedness and tameness: Differentialless geometry of plane curves, *Pattern Recog.* **31**, 1998, 607–622.
18. L. J. Latecki and R. Lakämper, Discrete approach to curve evolution, *Proc. of 20th DAGM Mustererkennung, Stuttgart, 1998.*
19. R. Lakämper, L. J. Latecki, and U. Eckhardt, Contour-based shape similarity, *Proc. SPIEs Conference on Vision Geometry San Diego, July 1998*, Vol. 3454.
20. L. J. Latecki and R. Lakämper, http://www.math.uni-hamburg.de/home/lakaemper/shape.
21. R. A. Melter, A. Rosenfeld, and P. Bhattacharya (Eds.), Vision geometry. *Contemporary Mathematics*, Vol. 119, pp. 169–195, Am. Math. Soc., Providence, 1991.
22. F. Mokhtarian and A. K. Mackworth, A theory of multiscale, curvature-based shape representation for planar curves, *IEEE Trans. Pattern Anal. Mach. Intell.* **14**, 1992, 789–805.
23. U. Ramer, An iterative procedure for the polygonal approximation of plane curves, *Comput. Graphics Image Process.* **1**, 1972, 244–256.
24. E. J. Pauwels, P. Fiddelaers, and F. Mindru, Fully unsupervised clustering using center-surround receptive fields with applications to colour-segmentation, in *Proc. of 7th Int. Conf. on Computer Analysis of Images and Patterns, Kiel, 1997*, pp. 17–24.
25. K. Siddiqi and B. B. Kimia, Parts of visual form: Computational aspects, *IEEE Trans. Patt. Anal. Mach. Intell.* **17**, 1995, 239–251.
26. K. Siddiqi, K. Tresness, and B. B. Kimia, Parts of visual form: Ecological and psychophysical aspects, in *Proc. of the IAPR's International Workshop on Visual Form, Capri, 1994*.
27. K. Siddiqi, K. Tresness, and B. B. Kimia, Parts of visual form: Psychophysical aspects. *Perception* **25**, 1996, 399–424.
28. A. W. M. Smeulders and L. Dorst, Decomposition of discrete curves into piecewise straight segments in linear time, *Contemporary Mathematics*, Vol. 119, pp. 169–195, Am. Math. Soc., Providence, 1991.
29. H. Tek, P. A. Stoll, and B. B. Kimia, Shocks from images: Propagation of orientation elements, in *Proc. of IEEE Conf. on Computer Vision and Pattern Recognition, Puerto Rico*, 1997, pp. 839–845.
30. Y. Uesaka, A new fourier description applicable to open curves, *Trans. IECE Japan A* **J67**, 1984, 166–173. [in Japanese]
31. L. Vaina and S. Zlateva, The largest convex patches: A boundary-based method for obtaining object parts. *Biol. Cybernet.* **62**, 1990, 225–236.
32. J. Weickert, A review of nonlinear diffusion filtering, in *Scale-Space Theory in Computer Vision* (B. M. ter Haar Romeny, *et al*., Eds.), pp. 3–28, Springer-Verlag, Berlin, 1997.
33. C. T. Zahn and R. Z. Roskies, Fourier descriptors for plane closed curves, *IEEE Trans. Comput.* **21**, 1972, 269–281.